

tric dipole transitions. Thus, we see that where  $\text{H}_2\text{O}$  has one allowed electric dipole transition  $\text{D}_2\text{O}$  has three. The molecule  $\text{HDO}$  has no multiplets; therefore, its spectrum will differ from  $\text{H}_2\text{O}$  and  $\text{D}_2\text{O}$ .

In  $\text{NH}_3$  we also find only a single electric dipole transition from the ground state  ${}^4P(sp^2)$  to the  ${}^4P(p^3)$  excited state. From the ground state  ${}^7D(sp^2)$  of  $\text{ND}_3$ , electric dipole transitions are allowed to the  ${}^7F(p^3)$ ,  ${}^7P(p^3)$ , and  ${}^7P(s^2p)$  excited states. Electric quadrupole selection rules allow transitions from the ground state to the  ${}^7S(sp^2)$  and  ${}^7S(s^3)$  excited states. The intermediate deuterides  $\text{ND}_2\text{H}$  and  $\text{NDH}_2$  would have spectra similar to  $\text{D}_2\text{O}$  and  $\text{H}_2\text{O}$ , respectively, and these would differ from  $\text{ND}_3$  and  $\text{NH}_3$ .

In  $\text{CH}_4$  there are no electric dipole allowed transitions from the  ${}^5S(sp^3)$  ground state. However, in  $\text{CD}_4$  we see that from the  ${}^9F(sp^3)$  ground-state electric dipole transitions are allowed to the

${}^9G(p^4)$ ,  ${}^9D(p^4)$ , and  ${}^9D(s^2p^2)$ , and electric quadrupole transitions are allowed to the  ${}^9P(sp^3)$  and  ${}^9P(s^3p)$ . The spectra of the intermediate hydrides would be similar to the corresponding di- or trideuteride or hydride, as the case may be.

Since the calculated protonic transition energies are of the same order of magnitude as electronic transition energies<sup>3</sup> and the calculated protonic intensities are about the same as the electronic intensities,<sup>4</sup> it would be difficult to distinguish a protonic transition from an electronic transition. The difference between the deuteronic structure and the protonic structure gives a way to support the existence of these postulated spectra. If transitions were found in a deuteride which did not appear in the hydride, these could not be electronic transitions because both molecules have similar electronic structures. A possible interpretation would be the differences in spectra described above.

\*Research sponsored by the U. S. Atomic Energy Commission under contract with the Union Carbide Corporation.

<sup>1</sup>I. L. Thomas, Phys. Rev. A 2, 728 (1970).

<sup>2</sup>I. L. Thomas, Chem. Phys. Letters 3, 705 (1969);

Phys. Rev. 185, 90 (1969).

<sup>3</sup>I. L. Thomas and H. W. Joy, Phys. Rev. A 2, 1200 (1970).

<sup>4</sup>I. L. Thomas, Phys. Rev. A 2, 72 (1970).

## Measurement of the $2^2S_{1/2}-2^2P_{3/2}$ Interval in Atomic Hydrogen\*

S. L. Kaufman,<sup>†</sup> W. E. Lamb, Jr., K. R. Lea, and M. Leventhal<sup>‡</sup>  
*Physics Department, Yale University, New Haven, Connecticut 06520*  
 (Received 15 June 1971)

An experiment is described in which the two transitions  $\alpha a(m_J = +\frac{1}{2} \rightarrow +\frac{3}{2})$  and  $\alpha b(m_J = +\frac{1}{2} \rightarrow +\frac{1}{2})$  were employed to measure the interval  $(\Delta E - S)_H$ . Hydrogen atoms in the metastable state are produced by bombarding molecular hydrogen with electrons within a waveguide in a magnetic field. An rf electric field in the guide induces electric dipole transitions from this state to the  $2P$  states, and the 1216-Å radiation produced in the decay of the  $2P$  state is detected. The frequency of the rf field is held constant, and the magnetic sublevels of the states involved are tuned by varying the magnetic field. When the resonance condition is met, the intensity of 1216-Å light increases. Precision measurements of signal versus magnetic field are fitted by least squares to a line-shape formula described in detail. Potential sources of systematic error and experimental searches for them are described. Small shifts are detected upon changing the electron-beam current and gas pressure, and an extrapolation is made to remove them. The weighted average of results from the two transitions is  $(\Delta E - S)_H = 9911.377(26)$  MHz. A comparison is made with other recent experiments which have measured the same interval.

### I. INTRODUCTION

The fine-structure intervals of the  $n=2$  states of deuterium were measured with high precision in the early 1950's. The  $2^2S_{1/2}-2^2P_{1/2}$  splitting  $s_D$  was measured by Triebwasser, Dayhoff, and Lamb,<sup>1</sup> and the  $2^2S_{1/2}-2^2P_{3/2}$  interval  $(\Delta E - s)_D$  by Dayhoff, Triebwasser, and Lamb.<sup>2</sup> These pre-

cision results were added to obtain the  $2^2P_{1/2}-2^2P_{3/2}$  interval  $\Delta E_D$ , for many years considered the best experimental source of a value<sup>3</sup> for the fine-structure constant  $\alpha$ . In the case of hydrogen, however, the  $(\Delta E - s)_H$  interval was not measured sufficiently accurately at that time to permit obtaining an independent value of  $\alpha$  having precision comparable to that from deuterium. In recent

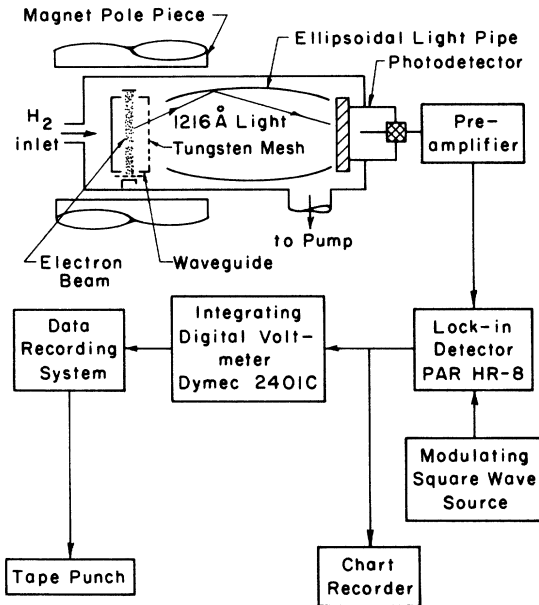


FIG. 1. Schematic diagram of experimental apparatus.

years, renewed experimental interest at various laboratories has led to improved results for fine-structure intervals in hydrogen.<sup>4-10</sup> The values for  $\alpha$  derived from these new fine-structure measurements are not in agreement with the previously accepted value, but instead are more consistent with those determined from the hyperfine structure of the hydrogen ground state<sup>11</sup> and the muonium ground state,<sup>12</sup> and from measurements on the ac Josephson effect.<sup>13</sup>

In our laboratory, we have measured two hydrogen transitions, both of which provide a value for the interval  $(\Delta E-s)_H$ . The two transitions are

$$\alpha a (2^2S_{1/2}(m_J = \frac{1}{2}) - 2^2P_{3/2}(m_J = \frac{3}{2}))$$

and

$$\alpha b (2^2S_{1/2}(m_J = \frac{1}{2}) - 2^2P_{3/2}(m_J = \frac{1}{2})) .$$

The results have already been reported in brief,<sup>14</sup> In the present paper we describe the details of the experimental method employed in this measurement and explain more fully the interpretation of the data. Finally, we compare our result with two other recent experimental measurements of  $(\Delta E-s)_H$ , and note the existence of an as yet unresolved disagreement between them.

## II. METHOD OF EXPERIMENT

Hydrogen atoms in the metastable  $2^2S_{1/2}$  states are produced inside a waveguide, between the poles of a magnet, as illustrated in Fig. 1. The metastables are produced by bombarding molecular

hydrogen with electrons at about 25 eV. A microwave field is applied to the atoms in the waveguide, and when a resonance condition is met, the mixing of *S* and *P* states by the rf field allows the excited atoms to decay with the emission of 1216 Å light. The light emitted in this process of "rf quenching" of the metastables, along with background light, is gathered by an ellipsoidal mirror (light pipe) and falls on a photodetector outside the magnet gap. The "signal" is defined as that part of the photocurrent which appears only when rf is applied. To extract the signal from the total photocurrent, the rf intensity is modulated and a phase-sensitive or "lock-in" detector is used. Measurements of the signal are made at several magnetic fields, and the resulting resonance curves are analyzed to find the energy separation of the two levels involved.

All previous precision measurements<sup>1,2,4,5</sup> of the  $n=2$  *S*-to-*P* intervals of atomic hydrogen have used an atomic-beam method. The regions of dissociation of molecular hydrogen, excitation to the 2*S* state, rf coupling to the 2*P* state, and detection of the beam were clearly separated. By contrast, the present experiment combines dissociation and excitation in one event leading to metastables traveling in all directions in the region in which the rf field is applied. The beam experiments measured the current of metastables reaching a metal surface, while now the light from their decay in the bombardment region is detected. It will be seen that the present experiment is much like microwave-optical experiments<sup>15-18</sup> on the short-lived states of H and He<sup>+</sup>. It resembles even more closely the experiments of Lamb and Skinner<sup>19</sup> and the later experiments of Novick and co-workers<sup>20,21</sup> and of Narasimham<sup>22</sup> on the  $2^2S_{1/2} - 2^2P_{1/2}$  interval in the  $n=2$  state of He<sup>+</sup>. As in all of these experiments, the atoms studied may be influenced by space-charge fields, stray fields of electron-gun electrodes, and collisions with ions, electrons, and neutral particles. Because of the great precision sought, estimates of the effects of all of these processes must be made, and experimental searches for systematic changes in the results must be undertaken.

## III. THEORY

The first part of this section deals with the working Hamiltonian and the means used to calculate energies, dipole matrix elements, and Stark shifts. Terms omitted from the working Hamiltonian are discussed briefly, and the significant ones estimated. Section III B develops a theory of the line shape in terms of a quenching function. Statistical distributions of velocity and other parameters are allowed for. A method is indicated whereby the experimentally measured dependence of signal on rf intensity can be used to obtain part of this quenching function.

## A. Energy Levels

The working Hamiltonian is taken directly from Lamb.<sup>23</sup> For  $S$  states, it is

$$\mathcal{H}_S = s + g_s \mu_B \vec{H} \cdot \vec{S} - g_I \mu_B \vec{H} \cdot \vec{I} + \Delta w \vec{I} \cdot \vec{S}, \quad (1)$$

while for  $P$  states,

$$\mathcal{H}_P = \frac{2}{3} \Delta E (1 + \vec{L} \cdot \vec{S}) + g_s \mu_B \vec{H} \cdot \vec{S} + g_I (1 - m/M) \mu_B \vec{H} \cdot \vec{L} - g_I \mu_B \vec{H} \cdot \vec{I} + w_P. \quad (2)$$

Here,  $s$  is the  $2^2S_{1/2} - 2^2P_{1/2}$  separation. The fine-structure interval  $2^2P_{3/2} - 2^2P_{1/2}$  is represented by  $\Delta E$ . The hyperfine energy operator for the  $P$  states is, in terms of the zero-field hyperfine splitting  $\Delta w$  of the  $2^2S_{1/2}$  state,

$$w_P = \left(\frac{3}{2}\right) \Delta w \langle r^{-3} \rangle [2\vec{I} \cdot \vec{L} + \left(\frac{1}{5}\right) g_s \times (4\vec{I} \cdot \vec{S} - 3\vec{I} \cdot \vec{L} \cdot \vec{S} - 3\vec{L} \cdot \vec{S} \vec{I} \cdot \vec{L})]. \quad (3)$$

Terms not included in this Hamiltonian have negligible effects on the energies, as discussed below.

Since the experimentally measured quantities are frequencies of atomic transitions instead of energies, and proton resonance frequencies instead of magnetic fields, there is an advantage in precision if all energies are expressed as frequencies, and the Zeeman (magnetic field dependent) terms of the Hamiltonian are calculated directly from the measured circular resonance frequency  $\nu_{\text{NMR}}$  of protons in water. This is done by using the relationship

$$\nu_{\text{NMR}} = g_I \mu_B H (1 - \sigma_{\text{H}_2\text{O}}) / \hbar \quad (4)$$

and the ratio  $g_s/g_p'$  of the gyromagnetic ratio of the free electron to that of the proton in water. For hydrogen, the Zeeman terms are

$$\begin{aligned} g_s \mu_B H / \hbar &= (g_s/g_p') \nu_{\text{NMR}}, \\ g_I \mu_B H / \hbar &= (g_s/g_p') (g_I/g_s) \nu_{\text{NMR}}, \\ g_I \mu_B H / \hbar &= (1 - \sigma_{\text{H}_2\text{O}})^{-1} \nu_{\text{NMR}}. \end{aligned} \quad (5)$$

The constant  $\sigma_{\text{H}_2\text{O}}$  allows for the diamagnetic shielding of the proton in water. The values of all constants used to evaluate the Hamiltonian are given in Table I.

In order to obtain all energy levels, dipole matrix elements, and Stark shifts in a simple way, the following procedure was used. The matrix of the working Hamiltonian for the 16 sublevels of  $n=2$  was evaluated in the  $Lm_L m_S m_I$  representation. A computer program based on Jacobi's iterative method was used to diagonalize the matrix, obtaining the eigenvectors as well as the eigenvalues. The eigenvectors were used to calculate the dipole matrix elements from a knowledge of their values in the  $Lm_L m_S m_I$  representation, and all eigenvalues and

dipole matrix elements were stored for later use in curve fitting.

To calculate Stark shifts due to an electric field  $\vec{E}$ , the original Hamiltonian matrix was modified by adding the matrix  $V = e\vec{E} \cdot \vec{r}$ . The diagonalization was then performed, and the resulting eigenvalues were compared with those found from the unperturbed Hamiltonian. In this way, Stark shifts were calculated and stored, for electric fields of 10 V/cm in each of two directions: parallel and perpendicular to the magnetic field. Stark shifts for other electric field strengths of the same order of magnitude vary as the square of the electric field.

To avoid errors in setting up the Hamiltonian matrix, the calculations were double checked by performing them in the  $FJLm_F$  representation.<sup>24</sup> This also gave an idea of the rounding error involved in the iterative diagonalization program. A further check was made by calculating the energies using perturbation theory.<sup>23</sup> Agreement among these three methods was within 0.002 MHz, which was taken as an estimate of rounding error. To obtain this agreement in the case of perturbation theory, it was necessary to include terms of order  $(\mu_B H / \Delta E)^2 \Delta w$  and  $(\Delta w / \Delta E)^2 \mu_B H$ . These terms alter the separation of hyperfine components of

TABLE I. Physical constants. The values given were assumed in all the data analysis. The error figures were not used, but are included here for convenience.

Symbol	Value
$S_H$	1057.77 ± 0.10 MHz <sup>a</sup> (Ref. 1)
$\Delta E_H$	10 968.61 ± 0.20 MHz <sup>a,b</sup>
$R_H/R_D$	0.999 728 0 <sup>c</sup>
$g_s$	2[1 + (1.159 622 ± 0.000 027) × 10 <sup>-3</sup> ] <sup>d</sup>
$g_s/g_p'$	658.227 59 ± 0.000 02 <sup>e</sup>
$m_e/M_p$	[(5.446 32 ± 0.000 18) × 10 <sup>-4</sup> ] (Ref. 3)
$\gamma/\hbar$	99.692 MHz <sup>f</sup>
$\sigma_{\text{H}_2\text{O}}$	[(25.6 ± 0.4) × 10 <sup>-6</sup> ] <sup>g</sup>
$\Delta w$	177.556 86 ± 0.000 05 MHz <sup>h</sup>

<sup>a</sup>These values were assumed at the outset, and the experimental results were applied as described in the section on data analysis.

<sup>b</sup>The value of  $\Delta E_D$  given in Ref. 2 was multiplied by  $R_H/R_D$  to obtain this value. This conversion is correct to better than one part per million, as can be seen from Ref. 3, Eq. (17).

<sup>c</sup>E. R. Cohen, Phys. Rev. **88**, 353 (1952).

<sup>d</sup>D. T. Wilkinson and H. R. Crane, Phys. Rev. **130**, 852 (1963). The correction to this value reported by A. Rich [Phys. Rev. Letters **20**, 967 (1968)] does not affect the results of the present experiment.

<sup>e</sup>E. B. D. Lambe, thesis (Princeton University, 1959) (unpublished) (quoted in Ref. 3).

<sup>f</sup>Reference 23, p. 269.

<sup>g</sup>N. F. Ramsey, *Molecular Beams* (Oxford U.P., London, England, 1963), p. 162.

<sup>h</sup>J. Heberle, H. Reich, and P. Kusch, Phys. Rev. **101**, 612 (1956).

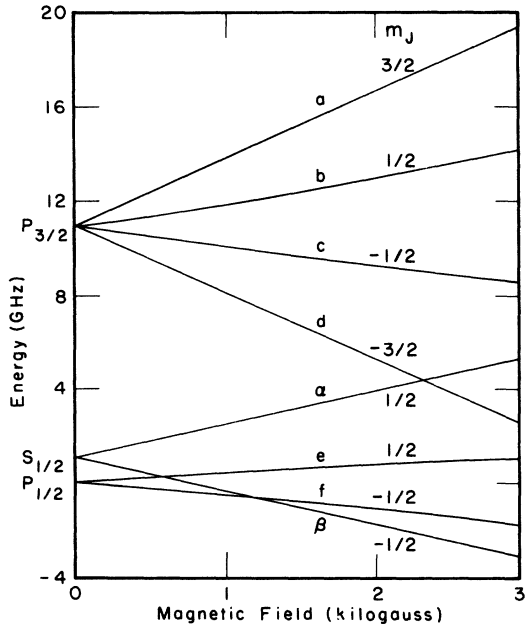


FIG. 2. Energies of the  $n=2$  states of hydrogen in a magnetic field, excluding hyperfine structure. The labels  $a, \dots, f, \alpha$ , and  $\beta$  are used in the text as abbreviations for the sublevels, following the usage of Lamb and Retherford (Ref. 27).

some of the resonance lines, without affecting apparent centers of the composite curves. The energies of the  $n=2$  levels are shown in Fig. 2, in the absence of hyperfine structure.

We have established the accuracy with which the

energies of the working Hamiltonian have been found. Terms omitted from this Hamiltonian will now be considered. The quadratic Zeeman effect increases the energies of all  $n=2$  levels by amounts on the order of 0.01 MHz.<sup>23</sup> The relativistic corrections<sup>25,26</sup> to the Zeeman energy have about the same magnitude. The  $P$  state hyperfine interaction  $w_P$  excludes terms<sup>24</sup> of similar magnitude which change the hyperfine splittings without affecting the centers of the observed composite resonances. The quadratic Zeeman and relativistic energies were calculated for each transition at the center of the observed resonance, and used to correct the experimental results after fitting to the line shape as calculated from the working Hamiltonian. The values of these corrections are included in Table II with the results.

#### B. Construction of Quenching Function

A simple model is needed to investigate the form of the "quenching curve" of signal versus rf intensity. This curve determines the form of saturation broadening of the resonance line. First, we consider its form in the case of a single velocity and uniform rf intensity. Let  $r$  metastable atoms per second, each with velocity  $v$ , be excited at point  $P$ . Assuming that all quenching processes are independent, let  $\mu$  be the probability per unit time that an atom is quenched by rf and  $\lambda$  be the probability per unit time that an atom is quenched by any other process. In the steady state, the rate of arrival of unquenched atoms at a distance  $L$  from  $P$  will be  $re^{-(\mu+\lambda)L/v}$ . The steady-state flux of

TABLE II. Summary of results and corrections. The  $\alpha c$  results were not incorporated into the final average, but are included for completeness. See text for details.

Transition	$\alpha a$	$\alpha b$	$\alpha c$
Number of runs	148	62	71
Frequency (MHz)	11970	9170	7430
Magnetic field at line center (gauss)	1465	1860	1090
Coefficients in Eq. (15):			
Pressure term (KHz mTorr <sup>-1</sup> )	+89.2(1.72)	-12.9(1.9)	+29.5 (105.0)
Current term (KHz mA <sup>-1</sup> )	+335(284)	-237(77)	+3.54(22) $\times 10^3$
Raw extrapolated result $(\Delta E - \delta)_0$ (MHz)	9911.402(18)	9911.394(10)	9911.027(050)
Corrections and uncertainties (MHz):			
NMR calibration	-0.058(12)	+0.015(03)	+0.039(008)
Relativistic energy	+0.019	-0.002	-0.012
Quadratic Zeeman energy	+0.001	+0.006	+0.003
Stray fields ( $\approx 2$ V/cm)	-0.001(02)	-0.006(06)	0.000
$\vec{v} \times \vec{H}$ Stark shift	(20)	(31)	(001)
Overlapping resonance	(10)	(30)	(300)
Computer rounding	(02)	(02)	(002)
Final results (MHz)	9911.363(31)	9911.407(45)	9911.057(304)
Weighted average (MHz)	9911.377(26)		

light leaving this path is proportional to  $r(1 - e^{-(\mu+\lambda)L/v})$ , the total number of metastables quenched per unit time along the path. The signal is proportional to the difference between the steady-state light flux when rf is applied and that when no rf is applied. When there is no rf,  $\mu = 0$ . The signal is therefore proportional to

$$F_0 = r e^{-\lambda L/v} (1 - e^{-\mu L/v}). \quad (6)$$

Lamb<sup>27</sup> obtained the quenching rates  $\lambda$  and  $\mu$  for the case of two levels  $n$  and  $m$  ( $S$  and  $P$  states, respectively) differing in energy by  $\hbar\omega_{nm}$  and coupled by an electric field. The  $P$  state is assumed to have a lifetime  $\tau = \gamma^{-1}$ , and the  $S$  state is assumed to be metastable with a lifetime much greater than  $\tau$ . In the present case, the effects of additional  $P$  levels may be incorporated by adding together the separate quenching rates calculated from the two-level solutions for each pair of levels. For a static electric field (or a motional field)  $\vec{E}_s$ , the result for the  $n$ th metastable sublevel is

$$\lambda_n = \sum_{m \neq n} \frac{\gamma |\langle m | e \vec{E}_s \cdot \vec{r} | n \rangle|^2}{\hbar^2 (\omega_{nm}^2 + \frac{1}{4} \gamma^2)}, \quad (7)$$

while for an oscillating field  $\vec{E}_0 \cos \nu t$  it is

$$\mu_n = \sum_{m \neq n} \frac{\gamma |\langle m | e \vec{E}_0 \cdot \vec{r} | n \rangle|^2}{4 \hbar^2 [(\omega_{nm} - \nu)^2 + \frac{1}{4} \gamma^2]}. \quad (8)$$

The latter expression is obtained by decomposing the cosine into its complex exponential form and discarding the nonresonating part. Besides this approximation, Eqs. (7) and (8) neglect a term of relative order  $(V/\hbar\gamma)^2$ , which for a perturbing field of 10V/cm is about  $10^{-5}$ . This term introduces no asymmetry and will not be considered further. Contributions to  $\lambda$  due to collisions with ions, electrons, and neutral molecules will be discussed later on in this paper.

In principle, the above model could be improved by allowing for complications such as the following: (i) The metastables are formed at all points within the electron beam. (ii) The atoms produced have different velocities. (iii) The rf intensity is not constant throughout the region observed. (iv) The distance  $L$ , beyond which the 1216 Å decay light is not collected, is not sharply defined. These factors might be incorporated by performing a numerical integration to derive appropriate expressions for the quenching function. To do this satisfactorily, more detailed knowledge would be required on the spatial dependence of each of the factors above. In the absence of such information, we adopted a less rigorous approach to the averaging. The *a posteriori* justification for this approach was the fact that line-center results were found to be insensitive to the exact form of the quenching function, so that a more elaborate treatment was not war-

ranted.

In the present approximation, then, the quenching function  $F$  is an average of  $F_0$  which allows for the factors (i)–(iv) through a weighting function  $W$ :

$$F(\lambda, \mu) = \langle F_0 \rangle = \int F_0 dW. \quad (9)$$

We now carry out this integration formally, expressing the average signal  $F$  in terms of some other averaged quantities. Let  $\psi = \lambda L/v$  and  $\varphi = \mu L/v$ , and let averaged quantities be indicated by angular brackets, e.g.,  $\langle \psi \rangle = \int \psi dW$ . In the approximation  $\psi \ll 1$ , the factor  $e^{-\psi}$  may be written as

$$e^{-\psi} [1 - (\psi - \langle \psi \rangle)].$$

The averaged signal in this approximation is proportional to

$$F_1 = r e^{-\langle \psi \rangle} [\langle 1 - e^{-\psi} \rangle - \langle (\psi - \langle \psi \rangle) (1 - e^{-\psi}) \rangle]. \quad (10)$$

The quantity  $\langle (\psi - \langle \psi \rangle) (1 - e^{-\psi}) \rangle$  vanishes for large rf intensity, where  $1 - e^{-\psi}$  is unity. Near zero rf intensity the expression in square brackets in Eq. (10) becomes

$$\langle \varphi \rangle \left[ 1 - \frac{\langle \psi \varphi \rangle - \langle \psi \rangle \langle \varphi \rangle}{\langle \varphi \rangle} \right].$$

The magnitude of the second term of this expression depends on  $\langle \psi \rangle$  and on the "sharpness" of the distribution  $W$ . For a single velocity, rf intensity, path length, etc., the term vanishes, and the low-power limit of  $F_0$  is recovered. If  $\psi$  and  $\varphi$  were independent, the averages could be performed independently, and the term would likewise vanish. This is not the case, since both  $\psi$  and  $\varphi$  depend on path length and velocity. Nevertheless, it is reasonable to expect that the term will be smaller than would be inferred from the value of  $\langle \psi \rangle$ . Furthermore, it depends on the magnetic field only to the extent that  $\psi$  does, and in most cases the term can be ignored even in precision curve fitting.<sup>28</sup> To see whether this was true for the resonances studied, a numerical calculation was made, in which the rf intensity was assumed uniform, the path lengths were assumed to be isotropically and uniformly distributed between 0.5 and 1.5 cm, and the empirical velocity distribution of Leventhal, Robiscoe, and Lea<sup>29</sup> was used. The only quenching included in  $\psi$  was that due to the motional electric field. Thus,  $\psi$  was proportional to  $vLH^2 \sin^2 \theta$ . The magnitude of the asymmetric term in Eq. (10) was found to be less than  $1 \times 10^{-4}$  across the resonance width. This resulted in a shift of the apparent line center of less than 3 kHz.

Apart from the term just discussed, the dependence of  $F_1$  on the rf intensity is contained in the factor  $\langle 1 - e^{-\psi} \rangle$ . This makes it possible to use the values of signal measured at different rf levels

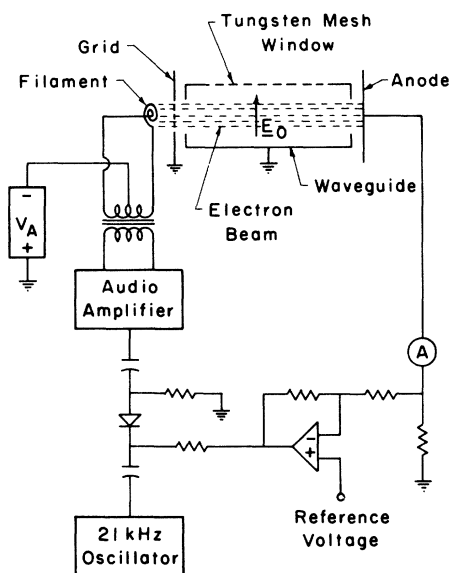


FIG. 3. Schematic diagram of electron gun and regulator.

to obtain a representation of this part of  $F_1$ . The data can be smoothed by fitting to a suitable function, as will be seen later. The composite nature of the observed signal, due to the hyperfine splitting, complicates this procedure slightly. However, if the magnetic field and frequency are chosen properly, the two hyperfine components of the  $S$  state will be quenched at nearly identical rates. Except for a change of scale, the observed quenching curve will then have the same form as that for a single level. A small contribution to the observed signal due to distant resonances involving metastables of the other  $m_J$  value may be taken as linear with the rf power.

#### IV. APPARATUS

##### A. Electron Gun and Regulator

The electron gun is shown schematically in Fig. 3. The filament is a flat spiral of about three turns of 0.010-in.-diam "non-sag" tungsten wire, heated by 21-kHz ac to prevent systematic shifts of the resonances due to its local magnetic field. For the  $\alpha b$  work, a flat Philips cathode 0.95 cm in diameter was used. This was heated indirectly by a bifilar heater, also using 21-kHz ac. The beam apertures are centered on the magnet axis, and currents to the electrodes indicate that the beam is well collimated by the magnetic field above 300 G. In the  $\alpha a$  work, the anode was kept at 200 °C to prevent accumulation of insulating deposits. Magnetic materials were carefully avoided in construction, and the final assembly was tested for magnetic impurities by observing its effect on the earth's field with the aid of a "fluxgate" mag-

netometer.

The current reaching the anode is held constant by a feedback circuit which changes the filament or heater current to compensate for changes in emission. This also keeps the anode current constant when the magnetic field is changed. The anode current stability over a 1-h period was found to be better than 0.02%, and the current changed by 0.015% when the magnetic field was increased from 1000 to 1500 G, producing no more than 3 kHz shift in the result.

##### B. Optical System

The ellipsoidal light pipe is made in three sections: the section within the magnet gap is oxygen-free high-conductivity (OFHC) copper, and the others are No. 316 stainless steel. The distance between foci is 28 in., and the minor axis is 3.84 in. The ends are truncated to permit placing the source and detector at the foci. The effectiveness of the light pipe at 1216 Å was estimated by comparing the photocurrent with the light pipe in place to that when it had been removed. Although it was difficult to be sure that conditions were accurately reproduced, it was concluded from these measurements that the light pipe increased the photocurrent by a factor of about 50. The photodetector alone subtends a solid angle of  $1.7 \times 10^{-3}$  sr about the center of the electron beam. The transparency of the tungsten mesh window in the waveguide is 90%. Thus, the effective solid angle of the detector is about  $7.5 \times 10^{-2}$  sr.

##### C. Photodetector and Preamplifier

The photodetector<sup>30</sup> consists of an ionization chamber filled with nitric oxide (NO) and carbon dioxide to partial pressures of 15 and 35 Torr, respectively. For the  $\alpha b$  and  $\alpha c$  work, the carbon dioxide filling was omitted. The magnesium fluoride window has a diameter of 1.25 in. The shell is maintained at a negative potential with respect to the anode, which is a 0.03-in.-diam Kovar rod. The spectral response is limited by the first ionization threshold<sup>31</sup> of NO at 1343 Å, and by the  $MgF_2$  window cutoff at about 1180 Å. Operated in the gas-gain mode,<sup>32</sup> this detector seemed sensitive to temperature changes, and its photocurrent was not proportional to light intensity, making it unsuitable for purposes of a precision experiment. In all of the work reported here, the device was used strictly as an ionization chamber without gain. Its quantum efficiency is stated by the manufacturer<sup>33</sup> to be 50% at 1216 Å, including window loss.

For the  $\alpha a$  and  $\alpha c$  work, the preamplifier was a simple dc-coupled source follower using a single MPF-103 field-effect transistor and a  $10^8$ -Ω input resistor. Later, for the  $\alpha b$  measurements, a pre-

amplifier of the Wing-Sanders<sup>34</sup> type was adopted, using a feedback resistance of  $10^9 \Omega$  and an Analog Devices model 141A operational amplifier.

The preamplifier is mounted inside a magnetic shield which also encloses the photodetector. This mounting permits a short wire connection to be made at the input, eliminating microphonic noise pickup. A permanent magnet, placed so as to produce a 100-G field at the detector and preamplifier, produced no observable change in the photocurrent. Since this field was many times stronger than the fringing field of the 12-in. magnet, it was concluded that the fringing field caused no significant systematic error.

#### D. Microwave System

The microwave system used for the  $\alpha\alpha$  measurements is shown schematically in Fig. 4. The klystron oscillator is phase locked by the synchronizer, which includes a crystal reference oscillator stable to a few parts in  $10^7$  per day. The microwave power enters the experimental region through a  $p-i-n$  diode modulator. A crystal detector samples the power in the waveguide and supplies a signal to the leveler, which compares this signal with a stable reference voltage and produces an error signal supplying just enough current to the modulator to keep the rf level constant during the "rf on" half of the modulation cycle. The leveler circuit is disabled during the other half of the cycle, and sufficient current is supplied to the modulator to obtain maximum (80 dB) attenuation. The ferrite isolator was found necessary in order to prevent momentary disruptions of the phase locking caused by the sudden changes in the impedance of the modulator when the rf power is switched off.

For the  $\alpha b$  measurements, the rf source was a sweep generator of the backward-wave oscillator type followed by a traveling-wave tube amplifier. A similar arrangement was employed for phase locking and modulation. The  $\alpha c$  measurements used a microwave system similar to that for the  $\alpha\alpha$  measurements, with the substitution of a lower-frequency klystron.

For frequency measurements, standard phase-locked transfer oscillator methods are used. The ultimate accuracy of the frequency measurement depends upon the frequency of the reference oscillator of a Hewlett-Packard 5245L frequency counter, which is calibrated periodically against WWVB's 60-kHz transmissions. Measurements at 12 GHz are accurate to about 100 Hz, far better than the requirements of this experiment.

A thermistor power meter measures the rf power reflected from the shorted end of the waveguide. This was found to be nearly equal to the forward power. The values of rf power quoted in this paper were measured while the rf was being

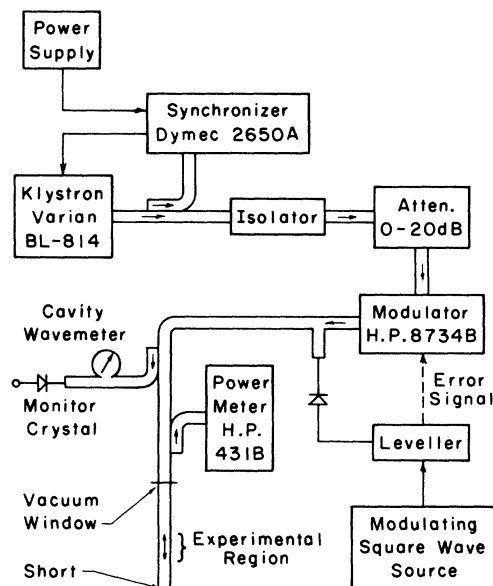


FIG. 4. Microwave system. The square-wave source is a divide-by-two circuit producing an accurate and constant 50% duty cycle.

100% square-wave modulated; thus, they are equal to one-half the actual reflected power during the "rf on" period.

#### E. Magnet and Power Supply

The iron-core magnet (Varian V-3603) has ring-shimmed pole pieces 12 in. in diameter with a gap of 3.75 in. Its power supply (Varian V-FR2503) uses a Hall-effect device in a feedback circuit to maintain the field at a value determined by the setting of a reference voltage. The field stability depends on the stability of the magnet temperature; under typical conditions, measurements showed the drift to be about 20 ppm in 30 min. Since field measurements were made at intervals of about 2 min, this drift was entirely acceptable. The homogeneity of the field in the volume of the electron beam is better than 10 ppm in the radial direction and 17 ppm along the axis, as measured by a movable proton resonance probe. This can change the measured resonance centers by no more than 6 kHz.

#### F. Magnetic Field Measurements

A space was provided on the magnet axis, outside the vacuum envelope, to receive a proton resonance probe. With the vacuum system open, a second probe could be placed in the position of the electron beam to determine a correction to the working probe's frequency at each magnetic field employed. This correction varied considerably with field, but was found to be stable in time

if the magnet was cycled within the region of the resonance to be studied. The cycling procedure was followed before each day's operation during the precision data taking.

The NMR system was a Magnion G-502 marginal oscillator, modified to reduce the field modulation amplitude to a value which permitted very reproducible settings to be made (to about 10 Hz at 6 MHz) with the aid of the built-in oscilloscope indicator. The water sample probes were supplied by Magnion.

#### G. Gas Supply and Pumps

Ordinary commercial-grade tank hydrogen is admitted to the system through a length of stainless-steel capillary tubing. The diameter and length of this tubing were adjusted by trial and error until a satisfactory range of pressures could be obtained by adjusting the tank regulator, a two-stage type with metal diaphragms. Since the leak rate is sensitive to temperature changes, the capillary was kept under the surface of a mineral oil bath.

The vacuum pump is a Welch 3102A pumping station incorporating a "turbomolecular" pump. This pump was chosen because of its ability to handle large volumes of gas at relatively high pressures, permitting a rapid flow rate in the system, to keep impurities from building up. It is connected to the vacuum envelope of the experimental apparatus by two 6-in.-diam stainless-steel bellows, with a heavy 6-in.-diam gate valve between them. The bellows and valve serve as a vibration filter.

The pressure is measured by means of a Pirani gauge, calibrated for air. Its readings were multiplied by the hydrogen correction factor of 0.43 to obtain the pressures quoted in this paper. These values were within 20% of the suitably corrected readings of an ionization gauge also connected to the system. The pressure in the region of the electron beam is thought to be within a factor of two of these corrected Pirani gauge readings.

The ultimate pressure with no hydrogen being admitted was measured by the ionization gauge to be  $6 \times 10^{-7}$  Torr. A Varian 974-0036 residual-gas analyzer showed that this background pressure consisted mainly of air and water vapor.

### V. SOURCES OF SYSTEMATIC ERROR

#### A. Effects of Varying the Magnetic Field

The electron beam operates in a magnetic field which is varied in order to study the atomic resonances. Even though the anode current is held constant electronically, it is possible that the rate of excitation of metastables varies systematically with the field, thus distorting the resonance. This would occur if the cross section for metastable production varied with field. A less fundamental, but

more plausible, source of such an "excitation asymmetry" is the spiraling and diffusion of the electrons and ions in the beam, resulting in a change with field of the effective bombarding current. In order to make a precision measurement, it is essential that the data be corrected in some way for any such asymmetry. By analogy with the atomic-beam technique of dividing the signal by the total beam intensity, this will be called "normalization." The details of the normalization scheme used in this experiment are presented in Sec. VII.

Other asymmetries are introduced into the resonance curve because of magnetic field variation. Of these, the rf matrix element variation and the motional quenching asymmetry are included in Eqs. (7) and (8). The possible asymmetry resulting from collisions is discussed in Secs. V C and V D, and an asymmetry related to the angular distribution of the decay radiation is described in Sec. V H.

#### B. Stark Effect

A macroscopic electric field in the experimental region will cause Stark shifts of the atomic levels. Such a field will be produced by the space charge of the electron beam and should depend on the beam current; thus an extrapolation to zero beam current is possible. (A maximum radial field of 6 V/cm is calculated for the periphery of a 200- $\mu$ A beam of 25-eV electrons of effective diameter 4 mm, under the extreme case of no neutralization by positive ions.) However, even if the effects of this field are removed by extrapolation, the possibility remains that charges on insulating surfaces or penetration of the field of the cathode into the interaction region could produce a field component independent of the beam current. The observed threshold for metastable excitation is 2-3 V above the theoretical value for typical beam currents, and furthermore, this threshold shift decreases as the beam current is reduced. This was taken as evidence that the field remaining after the beam is turned off must be small, and we have accordingly estimated it to be less than 2 V/cm. Extrapolation to zero beam current was made to allow for space charge fields and the Stark shift due to the possible 2 V/cm remaining field was included in the estimate of error.

The motional field  $\vec{v} \times \vec{H}/c$  causes Stark shifts whose values may be calculated and applied as a correction to the energies of Sec. III A. Recent experiments by Leventhal *et al.*<sup>29</sup> on the direct production of metastable hydrogen atoms by electron bombardment of molecular hydrogen have shown that the velocity spectrum contains two components having most probable velocities of  $8.3 \times 10^5$  and  $3 \times 10^6$  cm/sec, respectively. The thresholds for these components differ by about

10 eV, so that it is possible to produce just the "slow" component by using electrons of energy below the threshold for the "fast" component. The velocity distribution measured in that experiment may be used to calculate the Stark shifts for the present experiment. Assuming equal probability for all directions of motion, the average value of  $|\vec{v} \times \vec{H}/c|^2$  was found to be

$$\frac{2}{3} (1.02 \times 10^6 \text{ cm/sec})^2 H^2 / c^2.$$

This produces a Stark shift of 0.09 MHz for the  $\alpha a$  transition at 1465 G and 0.02 MHz for  $\alpha b$  at 1860 G.

#### C. Collisions with Charged Particles

Quenching of hydrogen metastables by collisions with charged particles has been discussed by several authors.<sup>35-37</sup> Purcell<sup>35</sup> gives a semiclassical method for estimating these effects in terms of an effective cross section for quenching, showing that for equal ion and electron densities, the effects of ions predominate. A calculation based on Purcell's results has been done here, in which the dependence of matrix elements and transition frequencies on the magnetic field was included. The result is that the quenching cross section changes slightly with field, having maxima near  $S$ - $P$  level crossings. According to this calculation, an ion density of  $5 \times 10^7 \text{ cm}^{-3}$ , corresponding to complete space-charge neutralization of a 100- $\mu\text{A}$  beam in the present experiment, would shift the  $\alpha a$  and  $\alpha b$  resonances each by 0.05 MHz.

#### D. Collisions with Neutral Molecules

The cross section for quenching of metastable hydrogen atoms by collisions with neutral hydrogen molecules has been estimated experimentally<sup>38</sup> to be  $0.7 \times 10^{-14} \text{ cm}^2$ . For atoms of velocity  $8.3 \times 10^5 \text{ cm/sec}$  and gas pressure  $10^{-3} \text{ Torr}$ , this large cross section implies a quenching rate  $\lambda$  of  $2 \times 10^5 \text{ sec}^{-1}$ , easily comparable to rf quenching rates in this experiment. If the quenching cross section does not vary with magnetic field or with the velocity of the encounter, no shift of the apparent line center will result. Estimates suggest that any such dependence must be very weak. Nevertheless, in view of the large quenching rate involved, even a small change could produce a significant shift. As will be seen, small shifts with pressure were detected, and the results were therefore extrapolated to zero pressure.

#### E. Doppler Effect

For an atom moving  $8.3 \times 10^5 \text{ cm/sec}$  in the direction of propagation of a plane electromagnetic wave of frequency 12 GHz, the Doppler shift is 0.33 MHz. Since the atoms in the present experiment move in all directions with equal probability,

the observed resonances are not shifted by this amount, but broadened symmetrically. The broadening adds to the natural line width  $\gamma$  only in quadrature for the observed resonance. Furthermore, the shorted waveguide produces standing waves which may be regarded as two waves traveling in opposite directions. Thus, even a single atom moving along the waveguide experiences two oscillating fields at frequencies symmetrically spaced about the applied frequency. For these reasons, the systematic error due to the Doppler effect is thought to be insignificant.

#### F. Cascade Effects

Transitions among the higher excited states induced by the rf field can, through cascading optical transitions, affect the production of  $2S$  states and of Lyman- $\alpha$  radiation. The effect depends on the excitation rates for the various states, and on the branching ratios for the decay. Resonances in the excited states have been observed in the present apparatus, and their presence has thus far prevented making precision measurements of the  $2^2S_{1/2}$ - $2^2P_{1/2}$  separation. Since the fine-structure intervals decrease as  $n$  increases, it is possible to avoid these resonances if the  $2^2S_{1/2}$ - $2^2P_{3/2}$  interval is studied. The  $n=2$  and some of the  $n=3$

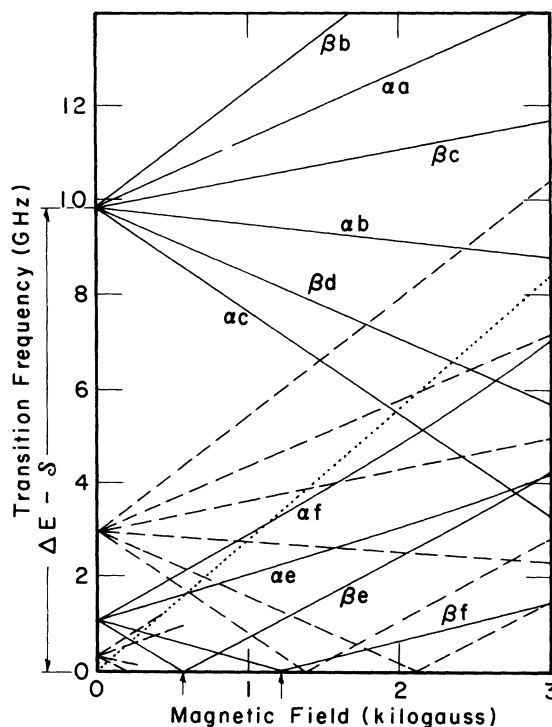


FIG. 5. Transition frequencies. Solid lines are  $n=2$  transitions. Dashed lines are  $n=3$  transitions observed through cascades. The dotted line shows the electron cyclotron frequency.

transition frequencies are shown in Fig. 5.

#### G. Escaping Metastables

If metastable atoms escape through the mesh window, they will contribute to the signal because of motional field  $\vec{v} \times \vec{H}/c$  and any rf or dc field existing outside the waveguide. Since the magnetic field decreases in the direction of the detector, this could cause a systematic error in the result. The rf field is likely to be small outside the guide, and the properties of the ellipsoidal light pipe are such that most of the collected light originates inside the waveguide. It has also been observed here that metastables are strongly quenched upon passing through such a tungsten mesh.

An experimental test for the effect of escaping metastables on the final result was made by placing a lithium fluoride window just outside the mesh window to make sure that no atoms could escape. The conclusion, based on about twenty  $\alpha\alpha$  runs, was that no significant error could be attributed to this effect. The lithium fluoride window was used for all of the  $\alpha b$  runs.

#### H. Angular Distribution of Decay Light

To the extent that the photodetector selects light emitted in one direction, a systematic change of the angular distribution of the decay light with magnetic field will cause an asymmetry in the observed resonances. Because of the spin-orbit interaction,  $P$  states with  $m_J = \pm \frac{1}{2}$  are linear superpositions of eigenstates with  $m_L = 0$  and  $\pm 1$ . The coefficients of these components are functions of magnetic field. The radiation pattern of decay from the  $m_L = 0$  component is that of a dipole oscillating along the magnetic field axis, while the pattern from each  $m_L = \pm 1$  component is that of a dipole oscillating in the plane perpendicular to the magnetic field, averaged over all orientations in the plane. Thus, the angular distribution of the radiation, for resonance signals involving these  $P$  states, does change with magnetic field.

The intensity of the light emitted perpendicular to the magnetic field ( $z$  axis) when the  $j$ th  $P$  state decays to the ground state  $g$  is proportional to  $\sum [|\langle g|x|j \rangle|^2 + |\langle g|z|j \rangle|^2]$ , where the sum is over sublevels of the ground state. The eigenvectors  $|j \rangle$  depend on the magnetic field. By evaluating this expression for magnetic field values across the resonance to be studied, a shift in the line center may be calculated. There are no shifts for  $m_J = \pm \frac{3}{2}$  states, since these states are independent of field. For the  $\alpha b$  resonances at the working field of 1860 G, the calculated shift is 0.19 MHz for the unbroadened line. This shift is almost entirely removed by a method of normalization to be described in Sec. VII.

The hyperfine interaction has only a small effect on the foregoing results, because the nuclear spin is almost completely decoupled from the total angular momentum. Its effect on the line centers can be calculated in a way similar to the foregoing, with the result that the additional shifts for  $\alpha\alpha$  and  $\alpha b$  are less than 1 kHz.

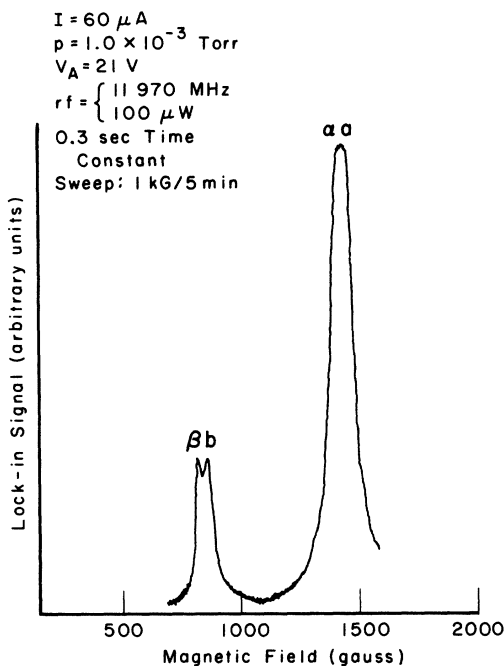
#### VI. CHOICE OF TRANSITIONS

It was decided that the first precision measurements should be made on the resonances least likely to be shifted by the sources of systematic error just discussed. The proximity of the  $\beta$  state to other levels in the range of magnetic fields available leads to large Stark shifts of  $\beta$  resonances due to motional and stray electric fields. The  $\alpha$  state is much less affected. The signals observed through cascades from higher states overlap most of the low-frequency transitions which would yield values for  $\delta$ , whereas the high-frequency transitions, yielding values of  $\Delta E - \delta$ , are well separated from such signals. Of these transitions,  $\alpha\alpha$  has the least natural asymmetry, and  $\alpha b$  has the largest rf matrix element. Both of these transitions were studied where overlap contributions to the resonance signal were small. The third high-frequency transition  $\alpha c$  was also studied, although known to be shifted significantly by the stronger nearby  $\beta d$  resonance.

#### VII. NORMALIZATION

In the atomic-beam experiments,<sup>1,2,4,5</sup> the signal was normalized by expressing it as a fraction of the maximum obtainable "beam flop." The maximum flop was determined by imposing a strong dc field on the beam, thus quenching substantially all of the metastables. In the present experiment, this is impossible, since applying a strong dc field in the experimental region would disturb the electron beam and cause a large change in light intensity not due to the quenching of metastables. It would seem that a large rf field could serve the purpose; rough calculations indicate that an rf level sufficiently high to produce essentially complete quenching would not affect the electron beam significantly. However, the present experiment also contends with the presence of  $\beta$  states. A high rf level will cause distant  $\beta$  resonances to overlap the desired  $\alpha$  resonance, adding an asymmetry to the normalizing signal. Since  $\beta$  states are appreciably quenched near the  $\beta e$  and  $\beta f$  crossings by fields which are not entirely known, as well as by collisions, it is desirable that their contributions to the normalizing signal be small.

The normalization method finally chosen was to use two rf levels, one quite low and the other sufficiently high to broaden the resonance considerably while by no means completely saturating it.

FIG. 6. Chart recorder tracing of  $\alpha\alpha$  and  $\beta\beta$  resonances.

Any asymmetry common to all metastable states does not appear in the ratio of the two signals, and neither signal contains appreciable  $\beta$  overlap. In terms of the resonance line formulas of Sec. III B, the normalized signal is

$$S_N = \frac{\sum F(\lambda_i, \mu_i)}{\sum F(\lambda_i, \mu_i')}, \quad (11)$$

where  $\mu_i$  and  $\mu_i'$  are the rf quenching rates for low and high rf levels, respectively. The sums extend over all metastable sublevels.

The only asymmetries remaining uncanceled in this formula are those that affect the various metastable sublevels differently. Some of these are calculable, such as the motional quenching asymmetry; others are related to space charge and to collisions, and their effects will be removed if the results are extrapolated to zero beam current and gas pressure. Different rates of excitation for different metastable sublevels would produce a noncanceling asymmetry also, but this requires an initial polarization of the hydrogen molecules or of the electron beam, which seems unlikely.

An alternate method which can be used to verify results obtained by this rf normalization scheme is the following. The signal is assumed to have a specific form of asymmetry besides its natural asymmetries, and a least-squares fit is used to find the value of the parameter which describes the asymmetry. A signal form of this kind is

$$S = A(1 + aH) \sum F(\lambda_i, \mu_i), \quad (12)$$

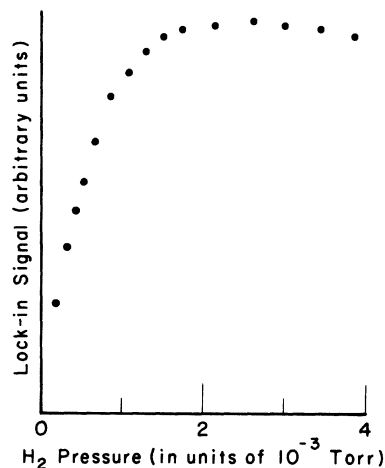
in which  $a$  is the asymmetry parameter and  $H$  is the magnetic field. The faults of this approach are evident: The assumed form of asymmetry may not be correct, and the first-order similarity of an asymmetry and a displacement of the line center make the results somewhat ambiguous. In spite of this, it has proved possible to use this method for a limited number of runs, and as will be seen, the results agree well with those of the more valid rf method. The asymmetry parameter is a useful by-product of this analysis.

### VIII. PRELIMINARY INVESTIGATIONS

#### A. Characteristics of Observed Resonances

##### 1. General

Figure 6 shows a typical chart-recorder trace of the  $\alpha\alpha$  and  $\beta\beta$  resonances at 11970 MHz, the frequency chosen for the final precision data on  $\alpha\alpha$ . The  $\beta\beta$  resonance is midway between the  $\beta e$  and  $\beta f$  crossings, and is susceptible to quenching by electric fields. The  $\alpha\alpha$  resonance, on the other hand, is relatively unaffected by fields large enough to quench most of the  $\beta$  states. The  $\alpha\alpha$  resonance height proved to be proportional to the electron-beam current up to about 300  $\mu A$ , but the  $\beta\beta$  height increased more slowly, so that the ratio of  $\beta\beta$  to  $\alpha\alpha$  resonance heights fell to one-half of its low-current value at 200  $\mu A$ . For this quenching to be due to the radial electric field of the space charge in the beam, the field should average about 6 V/cm, a value consistent with the estimate made in Sec. V B. However, this agreement should not be taken too seriously, since the discussion of Sec. VIII A 2

FIG. 7. Observed dependence of  $\alpha\alpha$  signal on hydrogen gas pressure.

suggests that there may be a slight *positive* space charge due to a superabundance of ions in the beam.

The signal depends on the gas pressure as shown in Fig. 7. Quenching of metastable hydrogen atoms by collisions with stationary gas molecules would result in a signal proportional to  $ne^{-n\sigma L}$ , where  $n$  is the number of molecules per unit volume,  $\sigma$  is the quenching cross section, and  $L$  is the path length. The observed peak is somewhat broader than the peak of this function, but this might be improved by averaging over the velocity distribution of the gas molecules. If  $L$  is assumed to be 1 cm, the cross section may be estimated from the pressure at the peak of the curve of Fig. 7 to be  $0.23 \times 10^{-14}$  cm<sup>2</sup>. The value estimated by Fite *et al.*<sup>38</sup> was about three times larger, but in view of the uncertainty in the measurement of pressure in the present experiment, and the need for estimating  $L$ , it is not felt that this represents disagreement.

To test the homogeneity of the rf field in the apparatus, attempts were made to observe resonances of the "wrong" polarization in each waveguide module. In spite of the presence of electron-beam apertures which were expected to distort the rf field, these resonances were weak when observed, and it was calculated that they could be neglected in making overlap corrections.

## 2. Excitation Curves

A study of the  $\alpha\alpha$  signal as a function of the applied electron beam potential  $V_A$  demonstrated, as shown in Fig. 8, a marked hysteresis effect. This persisted even after the electrode surfaces were cleaned, and is thought to be due to the following effect. When  $V_A$  is below the first ionization threshold of H<sub>2</sub>, the negative space charge in the electron beam produces a potential depression, reducing the actual electron energy. Ions can be formed only by increasing  $V_A$  sufficiently beyond the threshold to overcome this depression. When ions are produced, they are trapped in the potential well, and begin to neutralize it. The electron energy increases as a result, which in turn increases the ionization efficiency so that still more ions are formed. This "feedback" situation continues until limited by the rate of escape of ions. The rate of metastable production is also affected by the sudden increase in electron energy, hence the irreversible change in signal as  $V_A$  is increased. If  $V_A$  is now decreased, the ions remaining in the beam serve to keep the electron energy high, and ions continue to be produced fairly efficiently. However, the situation is stable only until  $V_A$  falls below a certain point, whereupon the negative space charge of the primary beam is restored. No hysteresis was observed in the  $\alpha b$  work, in which a somewhat different beam geometry was used.

## 3. Signal Strength and Signal-to-Noise Ratio

An electron beam of total current  $I$  and length  $L$ , operating in hydrogen gas of density  $n$  molecules per unit volume, produces metastable atoms at a rate given by  $r = (I/e)n\sigma L$  where  $e$  is the electronic charge and  $\sigma$  is the cross section for metastable production. If all of these atoms were quenched by the rf field, and a fraction  $\eta$  of this light ultimately produced electrons at the photodetector, the signal obtained would be  $S_{\max} = In\sigma L\eta$ . Lichten and Schultz<sup>39</sup> have estimated  $\sigma$  to be  $0.03\pi a_0^2$  to within a factor of 2. Using this value, and assuming a gas temperature of 300°K and an electron-beam length of 2.2 cm, the expected maximum signal is  $S_{\max} = 1.9 \times 10^{-4} Ip\eta$  where  $p$  is the gas pressure in millitorr.

With a bombarding current of 0.02 mA and a pressure of  $0.8 \times 10^{-3}$  Torr, the observed signal with a saturating rf level was  $1.9 \times 10^{-11}$  A. The expected signal  $S_{\max}$  is  $0.9 \times 10^{-11}$  A, using a value for  $\eta$  of  $3.0 \times 10^{-3}$  as calculated from the light pipe efficiency and photodetector quantum efficiency. In view of the uncertainties in the measurement of pressure and in Lichten and Schultz's<sup>39</sup> estimate of the cross section, this represents reasonably good agreement.

The signal is the difference of two very nearly equal values of the photocurrent, one measured with the rf field applied, and one without. Each of these measurements is influenced by shot noise and by thermal fluctuations in the measuring circuit. If the photocurrent  $i$  is averaged over time  $\tau$  for each measurement, the rms fluctuation in the signal will be  $i\sqrt{2}\tau^{-1/2}(e/i + 4kT/i^2R)^{1/2}$ , combining all four noise sources in quadrature. Here  $R$  is the input resistance of the measuring circuit,  $T$  is the absolute

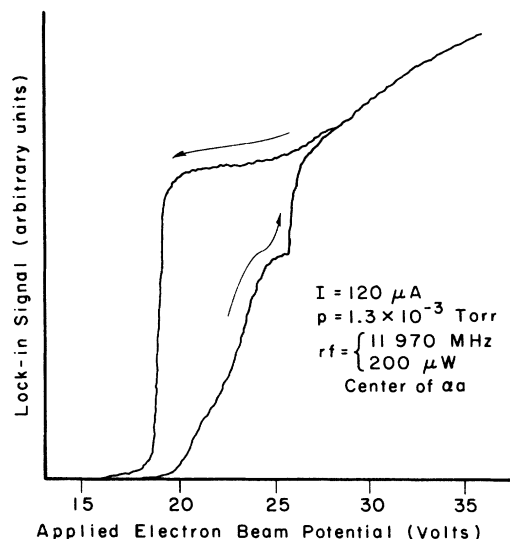


FIG. 8. Excitation curve, showing hysteresis phenomenon.

temperature,  $k$  is Boltzmann's constant, and  $e$  is the electronic charge. The signal is assumed to be a small fraction  $\rho$  of the total photocurrent. The ratio of signal to rms noise is then

$$S/N = \rho \tau^{1/2} [2(e/i + 4kT/i^2 R)]^{-1/2}. \quad (13)$$

In order to compare this result with the experimentally observed signal-to-noise ratio, the signal was measured repeatedly at the center of the  $\alpha\alpha$  resonance (11 970 MHz and 1465 G). The experimental conditions were pressure,  $0.75 \times 10^{-3}$  Torr; beam current,  $13 \mu\text{A}$ ; rf power,  $200 \mu\text{W}$ . The relevant parameters in Eq. (13) were:  $i = 1.6 \times 10^{-10}$  A,  $\rho = 7.1 \times 10^{-3}$ ,  $R = 10^8 \Omega$ ,  $T = 300^\circ\text{K}$ ,  $\tau = 5.0$  sec. The predicted signal-to-noise ratio under these conditions is 130. The observed signal-to-rms-noise ratio was 150 as determined from 28 successive measurements, in reasonable agreement with the prediction.

#### B. Search for Effect of rf on Electron Beam

The rf electric field acting on the electron beam might produce a change in light intensity which would be indistinguishable from the signal. If this false signal varied with magnetic field, the apparent line center would be shifted. Simple estimates suggest that any such effect should be extremely small, especially when the rf electric field is perpendicular to the magnetic field, but it was thought desirable to verify this experimentally. For this purpose a photomultiplier (EMR No. 542G-08-18) was substituted for the usual photodetector. Its threshold was  $2500 \text{ \AA}$ , and a sapphire filter<sup>40</sup> was used to limit the short-wavelength response to about  $1425 \text{ \AA}$ . The photomultiplier anode current was analyzed with the lock-in detector for a component due to the rf field. For a power level of  $0.3 \text{ W}$  at  $11\,970 \text{ MHz}$ , the fractional change in current due to the rf field was not measurable, but was less than  $10^{-6}$ . The working power levels for the final data did not exceed  $15 \text{ mW}$ , at which level the signal was about 1% of the ionization chamber's total photocurrent. On the basis of these figures it is estimated that the magnitude of any false signal due to this effect is less than  $10^{-5}$  of the desired resonance signal. This could cause shifts no larger than  $1 \text{ kHz}$  in the final result.

#### C. Experimental rf Quenching Curves

The signal was measured over a wide range of rf power  $P$ , with frequency and field chosen to make the intensities of the two hyperfine components of the given transition as nearly equal as possible. As mentioned in Sec. III B, the form of the quenching curve under these conditions is essentially the same as that for a single hyperfine component, except for a small linear part due to the distant  $\beta$  res-

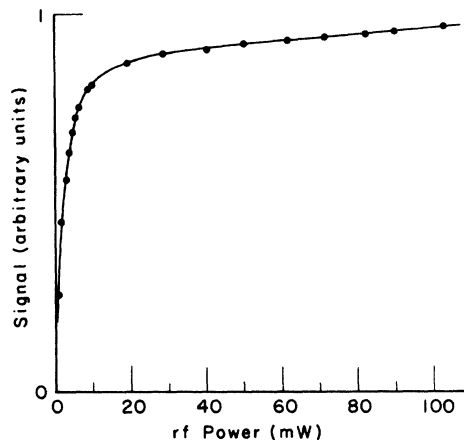


FIG. 9. rf quenching curve of Eq. (14) and experimentally measured points.

onance. Accordingly, the function  $N(1 - e^{-P/P_0}) + bP$  was fitted by least squares to the data, varying  $N$ ,  $P_0$ , and  $b$  to obtain the fit. The result was not satisfactory, and since the true quenching curve discussed in Sec. III B is an average of simple exponential forms, the next step was to approximate the averaging by allowing two such terms. The function  $N[A(1 - e^{-P/P_1}) + (1 - A)(1 - e^{-P/P_2})] + bP$  was fitted to the data, this time varying  $N$ ,  $A$ ,  $P_1$ ,  $P_2$ , and  $b$ . A good fit resulted, as shown in Fig. 9.

To find out whether the form of the quenching curve depended on gas pressure or bombarding current, ten runs of this kind of data were taken, at pressures ranging from  $0.79 \times 10^{-3}$  to  $2.1 \times 10^{-3}$  Torr, and at beam currents from  $16 \mu\text{A}$  to  $180 \mu\text{A}$ . The form of the curve is determined by  $A$  and the ratio  $P_1/P_2$ . Among the ten runs, no differences were observed in these quantities to within the statistical error. The value of  $b$  was in agreement with the value expected from the overlapping resonances.

To obtain a representation of  $F$  [Eq. (9)] from this experimental quenching curve,  $N$  is replaced by the factor  $r e^{-\langle \lambda L / v \rangle}$ , and the linear part  $bP$  is removed since  $F$  applies only to a single metastable state. The result is

$$F_1(\lambda, \mu) = r e^{-\langle \lambda L / v \rangle} [0.538(1 - e^{-0.2676(\mu L / v)}) + 0.462(1 - e^{-1.853(\mu L / v)})], \quad (14)$$

where average values of  $A$  and  $P_1/P_2$  from the ten runs have been used. The value of  $P_1$  is arbitrary, and was chosen to give Eq. (14) the same slope at zero rf power as the simple form  $e^{-\langle \lambda L / v \rangle}(1 - e^{-\langle \mu L / v \rangle})$  so that subsequent curve fitting would result in a fairly accurate value for the square of the rf electric field.

In the final data analysis, when this quenching

curve was used as part of the line shape, the influence of the form of the quenching curve on the final line center was tested by comparing the results obtained using this function with those obtained using the simple single exponential form. The influence on the line center was entirely negligible, owing to the high degree of symmetry of the  $\alpha a$  and  $\alpha b$  resonances.

#### IX. NORMALIZED PRECISION DATA AND ANALYSIS

The final result for  $(\Delta E - s)_H$  is based on 148 runs on the  $\alpha a$  transition at 11 970 MHz, and 62 runs on the  $\alpha b$  transition at 9 170 MHz. An additional 62 runs were taken on the  $\alpha c$  transition, but these proved to be subject to a large uncertainty owing to the overlapping  $\beta d$  resonance and were not incorporated into the final result. The experimental conditions of the runs were varied to discover any systematic dependence of the results on these conditions. First, a group of runs was taken in which each of the rf levels was varied over a wide range, and no systematic shifts were found. The next set of runs explored the dependence on beam current and pressure. In the measurement of  $\alpha a$ , beam currents were chosen between 50 and 300  $\mu A$ , while the  $\alpha b$  measurements used currents in the range 30 – 240  $\mu A$ . The pressure was varied between  $0.2 \times 10^{-3}$  and  $3.5 \times 10^{-3}$  Torr. Some dependence of the results on beam current and pressure was found. After sufficient runs were accumulated to determine the coefficients of these dependences, many more runs were taken under conditions where it was known that the pressure and beam current shifts were only 0.02 – 0.05 MHz. This procedure was carried out for both the  $\alpha a$  and  $\alpha b$  transitions.

After all runs were completed for a given transition, their results were analyzed together for the current and pressure shifts by means of a least-squares fit to a linear extrapolation formula:

$$(\Delta E - s)_{I,p} = (\Delta E - s)_0 + aI + bp. \quad (15)$$

Here,  $I$  is the beam current and  $p$  is the pressure. The value of  $(\Delta E - s)_0$  as determined by this fit is the "raw extrapolated result" shown in Table II. The individual runs were weighted equally since their statistical errors as determined from the individual fits to the line formula were not significantly different.

The data of a single run could be taken in about 15 min, and consisted typically of ten points taken near five different magnetic field values. The quantities measured for each data point were: the NMR frequency, the signal at each of the two rf levels, the lock-in amplifier zero offset, and the pressure. To take one data point, the NMR oscillator was set manually to the proton resonance frequency. Then a scanning cycle was initiated, which caused all of the measurements for that

point to be made in succession, and the values to be punched on paper tape. At the end of the scan, a motordriven control in the magnet power supply changed the magnetic field to the next value, and the system was ready for the next point. The order of the magnetic field settings was chosen to minimize the effect of any instrumental drifts on the line center. The signal measurements consisted of 10-sec integrations of the lock-in output. Actually, two such measurements were made at each of the two rf levels, alternating low and high rf, and the results were averaged later for each rf level. Table III presents the data and results for a sample  $\alpha a$  run.

The microwave frequency was measured occasionally between runs. It was found to be extremely stable, changing by no more than 1 kHz during all of the precision work. The rf power levels and the electron-beam current and gas pressure were also recorded between runs.

Each run was analyzed by means of a least-squares fit, using the line form given in Eq. (11). The empirical quenching function  $F_1$  given in Eq. (14) was used as a representation of  $F$ . The main resonance terms of  $\mu_i$  in both the numerator and denominator of Eq. (11) were modified by incorporating the averaged motional Stark shift  $s$  (Sec. V B) and a parameter  $\Delta$  which allowed the calculated transition frequency to be altered to fit the data. For example, the main resonance term in the numerator for the  $\alpha_+$  state was, for the  $\alpha a$  case,

$$\mu_{\alpha_+} = \frac{\gamma |\langle \alpha_+ | \vec{E}_0 \cdot \vec{r} | \alpha_+ \rangle|^2}{4\hbar^2 [(\omega_{\alpha_+} - \nu + s + \Delta)^2 + \frac{1}{4}\gamma^2]}. \quad (16)$$

The terms in  $\Delta$  and  $s$  were, of course, not included for the overlapping resonances, but only for the main resonance. The least-squares adjustment involved three parameters: the two rf levels and the frequency correction  $\Delta$ .

#### X. RESULTS

The results for the  $\alpha a$  and  $\alpha b$  transitions are shown in Table II. The values of  $(\Delta E - s)_{I,p}$  for all runs of a given transition were fitted by least squares to the extrapolation formula of Eq. (15). The value of  $(\Delta E - s)_0$  found from this fit is listed as the "raw extrapolated result." The corrections which were applied to this value are listed underneath. The NMR calibration is the correction for the probe position discussed in Sec. IV F. The relativistic energy and quadratic Zeeman energy were discussed in Sec. III A. The correction for stray fields allows for electric fields which may be present when the beam current is zero.

The figures of uncertainty shown for the raw extrapolated result are the standard deviation of the mean. The other uncertainty figures are not of a

TABLE III. Data of a typical run. Column 2 shows the measured NMR frequency and the probe position correction. Columns 3 and 4 are the lock-in signal at the two rf levels. The two values at each level are to be averaged. Column 5 is the zero offset, averaged for all points in the run as shown. The normalized signal for each point is (average low rf signal minus average zero)/(average high rf signal minus average zero). Experimental conditions were: pressure, 0.47 mTorr; rf power levels 0.3 and 6.0 mW; frequency 11970 001 MHz; beam potential 25V; beam current 120  $\mu$ A. The results of the least-squares fit for this run were:  $E_0^2(\text{low rf}) = 0.483 \text{ (V/cm)}^2$ ;  $E_0^2(\text{high rf}) = 7.52 \text{ (V/cm)}^2$ ; and  $(\Delta E - S)_{r,p} = 9911.396(145) \text{ MHz}$ .

Pt	NMR (MHz)	Signal (low rf)	Signal (high rf)	Zero	Normalized signal
1	6.278 868	-0.8010	+8.0757	-2.8934	0.18977
	+0.000 165	-0.8072	+8.0756		
2	6.019 855	-1.7649	+5.1034	-2.8783	0.13954
	+0.000 264	-1.7729	+5.1087		
3	6.681 424	-2.3638	+2.6642	-2.8839	0.09195
	+0.000 054	-2.3825	+2.6766		
4	5.855 987	-2.3971	+2.3617	-2.8825	0.09161
	+0.000 337	-2.4090	+2.3664		
5	6.500 197	-1.6255	+5.6925	-2.8789	0.14650
	+0.000 098	-1.6302	+5.6859		
6	6.019 074	-1.7792	+5.1091	-2.8824	0.13762
	+0.000 264	-1.7907	+5.0930		
7	6.681 394	-2.3713	+2.6770	-2.8892	0.09177
	+0.000 054	-2.3753	+2.6815		
8	5.861 778	-2.3889	+2.4474	-2.8813	0.09302
	+0.000 334	-2.3862	+2.4555		
9	6.499 088	-1.6200	+5.7163	-2.8815	0.14672
	+0.000 098	-1.6236	+5.7181		
10	6.258 454	-0.7968	+8.0672	-2.8865	0.19047
	+0.000 172	-0.7964	+8.0820		
				av zero = -2.8839	

statistical nature, but in estimating them an attempt was made to give realistic 68% confidence intervals so that when summed in quadrature together with the statistical standard deviation, the resulting figure could be treated as 1 standard deviation for purposes of combination and comparison with other experiments.

The uncertainty listed for the  $\vec{v} \times \vec{H}/c$  Stark shift arises from uncertainty in the assumed velocity distribution. The strength of the overlapping  $\beta$  resonance also depends on the velocity, and is subject to further uncertainty because of the need to estimate the distance of travel  $L$  and magnitude of any stray electric field.

The results for the  $\alpha c$  transition are included in Table II for completeness. Because of the large uncertainty due to the strongly overlapping  $\beta d$  resonance, these results were not used in the final average. It would be possible to study  $\alpha c$  at higher magnetic fields where the  $\beta d$  overlap is somewhat less important, but at these fields the motional Stark shift and the motional quenching of  $\alpha$  states become large. Also, transitions among states of higher principle quantum number are observed in

this region through cascades. The  $\alpha c$  transition was therefore abandoned in favor of  $\alpha a$  and  $\alpha b$ , whose interpretation is more straightforward.

Nine unnormalized  $\alpha a$  runs, including one 24-point panoramic and eight of the usual ten-point runs, were taken under conditions typical of the normalized data. Equation (12) was fitted to each of these runs by least squares, again using  $F_1$  as a representation of  $F$ , and treating the main resonance terms just as they were treated for the normalized data. The result for these nine runs,

TABLE IV.  $(\Delta E - S)$  in H,  $n=2$ . The figures of uncertainty quoted in this table are one standard deviation for the experimental results, and a "limit of error" for the theoretical result of Appelquist and Brodsky (Ref. 41). These authors used  $\alpha^{-1} = 137.03608$  in their calculations.

$(\Delta E - S)$ (MHz)	Reference
9911.12 $\pm$ 0.22	(Ref. 41)
9911.173 $\pm$ 0.042	(Ref. 7)
9911.250 $\pm$ 0.063	(Ref. 9)
9911.377 $\pm$ 0.026	Present experiment

after making the appropriate corrections, was 9911.347 (49) MHz, in agreement with the value obtained from the normalized data. The asymmetry parameter in Eq. (12) was found to be quite significant, amounting to a 4% change in signal strength across the resonance width. This would produce an apparent shift of about 1 MHz in the line center had it not been taken into account. The high-field side of the resonance is stronger than it would be if there were no asymmetry. The unnormalized data were not incorporated into the final result.

#### XI. DISCUSSION

After this work was completed, atomic-beam measurements of  $(\Delta E - s)_H$  were reported by Cosens and Vorburger<sup>7</sup> and by Shyn, *et al.*<sup>9</sup> It was thought desirable to publish details of our experiment at this time so that a better comparison between the methods could be made. Table IV lists the three most recent experimental values for  $(\Delta E - s)_H$ , and also shows the current theoretical value for this interval obtained by Appelquist and Brodsky.<sup>41</sup> The agreement between the two atomic-beam results (second and third lines of Table IV) is not surprising since the methods used were quite similar. The discrepancy between these results and those of the present work is as yet unexplained. We believe it arises from some difference between the experimental methods. Such differences include the following.

(i) The metastable hydrogen atoms are produced by a one-step molecular excitation and dissociation process, instead of the stepwise method used in the atomic beam experiments.

(ii) The fine-structure transitions are detected by observation of the optical decay radiation from the short-lived  $2P$  state, rather than by detection of the surviving metastable atoms in the beam.

(iii) The measurement is carried out in the perturbing presence of electrons, ions, and hydrogen molecules, and in the vicinity of walls which may have charge accumulations on insulating patches. (An explanation based on these perturbations must describe a residual shift after extrapolation to zero current and gas pressure.)

The items on the above list reveal the substantial differences between our experiment and the atomic-beam experiments. At the outset, we felt confident in our ability to analyze the unique aspects of our experiment, and by a combination of theoretical estimates and experimental tests, to narrow down the associated uncertainties. In view of the discrepancy which has since emerged, we have reconsidered the

possibilities for error in our experiment. This reexamination has yielded no specific item that may be at fault, although some suggestions that might be described as speculative have occurred to us. One example is the possible influence of the microwave and magnetic fields on the details of the molecular dissociation process, by which the metastable atoms are created. Another example is based on the fact that the optical detector responds not only to Lyman- $\alpha$  light, but also to a portion of the uv spectrum of molecular hydrogen, within the range 1180–1340 Å. A microwave transition in *molecular* hydrogen might conceivably occur, and contribute a "spurious" signal to the atomic hydrogen resonance line under study. However, the test described in Sec. VIII B already rules out the existence to any important extent of such signals in the uv between 1425 and 2500 Å. A third possible source of error may lie in the Stark shift due to a residual electric field in the interaction region. After making the extrapolations for the space-charge field versus gas pressure and beam current, there may exist a residual field arising perhaps from charges accumulated on insulating patches on the interior walls of the interaction region. The evidence discussed in Sec. V B suggests that any residual field is small, not exceeding 2 V/cm. The corresponding uncertainties due to this are small, and have been included in Table II. Yet another possibility has been raised by one of the present authors, who noted<sup>42</sup> that several hydrogen fine-structure measurements appeared to show a linear dependence on the magnetic field at which the measurements were made. Although the statistical significance of this dependence is doubtful, the observation causes some uneasiness, and prompts speculation on the sufficiency of the theory of the Zeeman effect.

We feel that further hypothesizing in these pages should be foregone, and instead hope for an eventual resolution of the discrepancy and reconciliation of results.

#### ACKNOWLEDGMENTS

The authors acknowledge the valuable assistance rendered by Dr. D. L. Mader, Dr. R. R. Jacobs, and Dr. W. H. Wing in many aspects of this research. The advice of R. J. Blume on electronic instrumentation was particularly helpful. In addition, we are grateful to several members of the staff of the Yale University physics department machine shop, under the direction of A. Disco, for the careful construction of a variety of items, including the very beautiful ellipsoidal light pipe.

\* Research supported in part by the U. S. Air Force Office of Scientific Research under AFOSR Grant No. 249-67.

† Present address: I. Physikalisches Institut der Uni-

versität Heidelberg, Heidelberg, Germany.

‡ Present address: Bell Telephone Laboratories, Murray Hill, N. J. 07974.

<sup>41</sup>S. Triebwasser, E. S. Dayhoff, and W. E. Lamb, Jr.,

- Phys. Rev. 89, 98 (1953).
- <sup>2</sup>E. S. Dayhoff, S. Triebwasser, and W. E. Lamb, Jr., Phys. Rev. 89, 106 (1953).
- <sup>3</sup>E. R. Cohen and J. W. M. DuMond, Rev. Mod. Phys. 37, 537 (1965).
- <sup>4</sup>R. T. Robiscoe, Phys. Rev. 138, A22 (1965).
- <sup>5</sup>B. L. Cosens, Phys. Rev. 173, 49 (1968).
- <sup>6</sup>Harold Metcalf, J. R. Brandenberger, and J. C. Baird, Phys. Rev. Letters, 21, 165 (1968).
- <sup>7</sup>B. L. Cosens and T. V. Vorburger, Phys. Rev. A 2, 16 (1970).
- <sup>8</sup>R. T. Robiscoe and T. W. Shyn, Phys. Rev. Letters 24, 559 (1970).
- <sup>9</sup>T. W. Shyn, T. Rebane, R. T. Robiscoe, and W. L. Williams, Phys. Rev. A 3, 116 (1971).
- <sup>10</sup>*Proceedings of the International Conference on Precision Measurement and Fundamental Constants*, edited by D. N. Langenberg and B. N. Taylor, Natl. Bur. Std. (U.S.) Misc. Publ. No. 343 (U.S. GPO, Washington, D.C., 1971). Reports by the authors of Refs. 6-9 and the present authors may be found in this volume.
- <sup>11</sup>J. E. Nafe and E. B. Nelson, Phys. Rev. 73, 718 (1948); S. B. Crampton, D. Kleppner, and N. F. Ramsey, Phys. Rev. Letters 11, 338 (1963); R. H. Vessot *et al.*, IEEE Trans. Instr. Meas. IM-15, 165 (1966).
- <sup>12</sup>P. A. Thompson, J. J. Amato, P. Crane, V. W. Hughes, R. M. Mobley, G. zu Putlitz, and J. E. Rothberg, Phys. Rev. Letters 22, 163 (1969); R. DeVoe, P. M. McIntyre, A. Magnon, D. Y. Stowell, R. A. Swanson, and V. L. Telegdi, *ibid.* 25, 1779 (1970). See also Ref. 10.
- <sup>13</sup>(a) W. H. Parker, B. N. Taylor, and D. N. Langenberg, Phys. Rev. Letters 18, 287 (1967); (b) B. N. Taylor, W. H. Parker, and D. N. Langenberg, Rev. Mod. Phys. 41, 375 (1969); (c) T. F. Finnegan, A. Denenstein, and D. N. Langenberg, Phys. Rev. Letters 24, 738 (1970).
- <sup>14</sup>S. L. Kaufman, W. E. Lamb, Jr., K. R. Lea, and M. Leventhal, Phys. Rev. Letters 22, 507 (1969); 22, 806E (1969). See also Ref. 10.
- <sup>15</sup>W. E. Lamb, Jr. and T. M. Sanders, Jr., Phys. Rev. 119, 1901 (1960).
- <sup>16</sup>L. R. Wilcox and W. E. Lamb, Jr., Phys. Rev. 119, 1915 (1960).
- <sup>17</sup>M. Leventhal, K. R. Lea, and W. E. Lamb, Jr., Phys. Rev. Letters 15, 1013 (1965); D. L. Mader, M. Leventhal, and W. E. Lamb, Jr., Phys. Rev. A 3, 1832 (1971).
- <sup>18</sup>K. R. Lea, M. Leventhal, and W. E. Lamb, Jr., Phys. Rev. Letters 16, 163 (1966); R. R. Jacobs, K. R. Lea, and W. E. Lamb, Jr., Phys. Rev. A 3, 884 (1971).
- <sup>19</sup>W. E. Lamb, Jr. and M. Skinner, Phys. Rev. 78, 539 (1950).
- <sup>20</sup>R. Novick, E. Lipworth, and P. F. Yergin, Phys. Rev. 100, 1153 (1955).
- <sup>21</sup>E. Lipworth and R. Novick, Phys. Rev. 108, 1434 (1957).
- <sup>22</sup>M. A. Narasimham, thesis (University of Colorado, 1968) (unpublished); M. A. Narasimham and R. L. Strombotne, Phys. Rev. A 4, 14 (1971).
- <sup>23</sup>W. E. Lamb, Jr., Phys. Rev. 85, 259 (1952). The correction to Eq. (184) of this reference noted by Robiscoe in Ref. 46 of Ref. 4 was included in our perturbation calculations mentioned in Sec. III A.
- <sup>24</sup>S. J. Brodsky and R. G. Parsons, Phys. Rev. 163, 134 (1967).
- <sup>25</sup>G. Breit, Nature 122, 649 (1928).
- <sup>26</sup>H. Margenau, Phys. Rev. 57, 383 (1940).
- <sup>27</sup>W. E. Lamb, Jr. and R. C. Retherford, Phys. Rev. 79, 549 (1950).
- <sup>28</sup>R. T. Robiscoe [Phys. Rev. 168, 4 (1968)] discusses a case in which  $\langle\psi\rangle$  is both large and asymmetric.
- <sup>29</sup>M. Leventhal, R. T. Robiscoe, and K. R. Lea, Phys. Rev. 158, 49 (1967).
- <sup>30</sup>See, e.g., J. A. R. Samson, *Techniques of Vacuum Ultraviolet Spectroscopy* (Wiley, New York, 1967), pp. 245 ff.
- <sup>31</sup>J. O. Sullivan and A. C. Holland, NASA Report No. CR-317, Washington, D. C., 1966, p. 114 (unpublished).
- <sup>32</sup>T. A. Chubb, NRL Report No. 4814, 1956 (unpublished).
- <sup>33</sup>Melpar, Inc., Falls Church, Va. 22046.
- <sup>34</sup>W. H. Wing and T. M. Sanders, Jr., Rev. Sci. Instr. 38, 1341 (1967).
- <sup>35</sup>E. M. Purcell, Astrophys. J. 116, 457 (1952).
- <sup>36</sup>M. J. Seaton, Proc. Phys. Soc. (London) 68, 457 (1954).
- <sup>37</sup>L. R. Wilcox and W. E. Lamb, Jr., Ref. 16, Appendix III C.
- <sup>38</sup>W. L. Fite, R. T. Brackman, D. G. Hummer, and R. F. Stebbings, Phys. Rev. 116, 363 (1959).
- <sup>39</sup>W. Lichten and S. Schultz, Phys. Rev. 116, 1132 (1959).
- <sup>40</sup>J. A. R. Samson, Ref. 30, Chap. 6.
- <sup>41</sup>T. Appelquist and S. J. Brodsky, Phys. Rev. A 2, 2293 (1970). *Footnote added in proof.* G. W. Erickson [Phys. Rev. Letters 27, 780 (1971)] computes  $(\Delta E - S)_H$  to be  $9911.123 \pm 0.031$  MHz.
- <sup>42</sup>S. L. Kaufman, in Ref. 10.